

Supplementary Appendix

Contents

CONTENTS	1
LIST OF INVESTIGATORS AND CONTRIBUTIONS	3
SUPPLEMENTAL TEXT	4
S1 – EXPERIMENTAL PROCEDURES	4
S1.01 – CLINICAL PROTOCOL AND STUDY PARTICIPANT	4
S1.02 – EEG MOTOR IMAGERY TEST	4
S1.03 – MULTI-MODAL MRI-BASED MOTOR LOCALIZATION.....	5
S1.04 - SURGICAL PLANNING	5
S1.05 - IMPEDANCE MEASUREMENT.....	6
S1.06 - BRAIN-COMPUTER INTERFACE TRAINING PARADIGMS	6
S1.07 – DAILY ASSESSMENT TASK.....	7
S1.08 – DEEP LEARNING BASED HAND TRAJECTORY TRACING.....	8
S2 – RIEMANNIAN DECODER	8
S2.01 - SPATIO-SPECTRAL RIEMANNIAN GEOMETRY DECODING METHOD.....	8
S2.02 - CONTROL DECODING METHODS.....	10
S2.03 - DECODING CONTINUOUS GRASPING STATES USING HIDDEN MARKOV MODEL	11
S2.04 - MODEL TRAINING AND EVALUATION	11
S3 - OFFLINE ANALYSIS OF EEG/ECOG DATA	12
S3.01 - COMPARISON OF THREE TYPES OF BRAIN ELECTROPHYSIOLOGY RECORDINGS	12
S4 – ELECTROPHYSIOLOGICAL AND NEUROLOGICAL ASSESSMENT OF REHABILITATION	13
S4.01 – SEP MEASUREMENT.....	13
S4.02 – NEUROLOGICAL SCALES MEASUREMENT	14
SUPPLEMENTAL FIGURES	15
FIGURE S1 MRI SCANS OF THE PATIENT'S HEAD AND NECK.....	15
FIGURE S2 fMRI LOCALIZATION TASK AND SURGICAL PLANNING.....	16
FIGURE S3 BRAIN-COMPUTER INTERFACE DECODING METHODS.....	17
FIGURE S4 ILLUSTRATION OF HMM DECODING.....	18
FIGURE S5 CALIBRATION AND TRAINING PARADIGMS.....	19
FIGURE S6 EVOLUTION OF EPIDURAL ECoG FEATURE DISTRIBUTION DURING LONG-TERM USE.....	20
FIGURE S7 EMG NOISE PATTERN.....	21
FIGURE S8 AVERAGE SOMATOSENSORY EVOKED POTENTIAL (SEP) WAVEFORMS.....	22

FIGURE S9 PNEUMATIC HAND KEYPOINT DETECTION MODEL.....23

SUPPLEMENTAL TABLES 24

TABLE S1: ISNCSCI SCORES.....24

TABLE S2: P-VALUES FOR INCREASES IN AVERAGE AMPLITUDES.....25

TABLE S3: ARAT SCORES26

TABLE S4: TRAINING SESSIONS.....27

REFERENCE..... 33

List of investigators and contributions

List of investigators (authors):

1. Dingkun Liu*
2. Yongzhi Shan*
3. Penghu Wei*
4. Wenzheng Li
5. Honglai Xu
6. Fangshuo Liang
7. Tao Liu
8. Guoguang Zhao
9. Bo Hong

* These authors contributed equally

Author contributions:

Supplemental Text

S1 – Experimental procedures

S1.01 – Clinical Protocol and Study Participant

This study was approved by the ethics committee of Xuanwu Hospital of Capital Medical University in April 2023 and registered for international clinical trials of implanted medical devices (NCT05920174) to conduct research on the implanted closed-loop brain-computer interface system (NEO). The surgery was performed at Xuanwu Hospital, with other related studies conducted at Tsinghua University and the patient's home. Our study includes three main phases: preoperative functional screening, surgery, an one-month calibration and adjustment period, and an eight-month BCI assisted active rehabilitation training period. The rehabilitation training involved a total of 100 sessions, each lasting 1-3 hours, tailored according to the patient's progress and health condition. In the 9th month, the training load was doubled to maximize the patient's recovery outcomes (Table S4).

The participant is a male in his 50s who sustained a spinal cord injury more than 10 years due to a car accident. The participant signed a written informed consent before participation. Moreover, the participant gave his consent for the material depicting himself to appear in the contribution and to be published in the journal and associated works without limit on the duration of publication, in any form or medium.

Before the surgery, the patient underwent a neurological impairment assessment, currently diagnosed as a complete C4 spinal cord injury (ASIA-A, Table S1). The patient's muscle tone was rated at level 2-3 on the Modified Ashworth Scale (MAS), indicating an increase in muscle tone that affects passive movement within the range of motion. The patient reported taking Baclofen (10mg/day) and Pregabalin (75mg/day) to relieve spasms at the sixth month post-surgery. This symptom has persisted since the injury and is unrelated to the BCI implant.

S1.02 – EEG Motor Imagery Test

The EEG data of the patients were recorded using a 20-channel 10-20 EEG system cap (Pony, Neuracle). To eliminate interference from electromyographic (EMG) signals, only 12 electrodes located at the center area were selected for the study (F3, Fz, F4, C3, Cz, C4, P3, Pz, P4, O1, Oz, O2), with CPz and AFz chosen as the reference and ground, respectively. The sampling rate was set to 1000 Hz.

The EEG motor imagery assessment paradigm involves both the left and right hands, with each round consisting of 15 trials. Each trial includes 5 seconds of movement, feedback (10 seconds for success, 2 seconds for failure), and 10 seconds of rest. Two rounds will be performed for each

hand. At the beginning of the experiment, a cross will appear in the center of the screen for 10 seconds, during which the participant is instructed to focus on the cross and remain calm. After this period, the actual task begins. When the movement phase starts, an arrow pointing left or right will appear in the center of the screen, indicating left-hand or right-hand movement, respectively. A text prompt will also appear above the screen saying, "Imagine left-hand/right-hand movement." After 5 seconds, feedback is provided based on the system's evaluation of the participant's motor imagery EEG during that time. If successful, a celebratory animation will play, and a pneumatic hand will perform a single grasp and release action, lasting 10 seconds. If unsuccessful, a 2-second encouragement animation will be shown. Following this, there will be a 10-second rest period, during which an image of a teacup will appear on the screen with the text "Rest, relax, stay calm," and the participant will be asked to remain relaxed. Throughout the experiment, the participant is required to sit quietly in a wheelchair, focus on the screen, and wear the pneumatic hand device. When the corresponding prompt appears on the screen, the participant begins the associated task.

S1.03 – Multi-modal MRI-based Motor Localization

Before the implantation surgery, the subject underwent a head MRI on a 3.0T scanner (Siemens, Prisma) to locate brain areas associated with hand sensory and motor functions. Functional MRI (fMRI) was acquired using a gradient echo planar imaging (EPI) sequence with the following parameters: matrix size 100×100, resolution 2×2×2 mm³, repetition time (TR) 2 s, echo time (TE) 30 ms. The scan covered the entire brain with 72 slices. T1-weighted MRI structural images were acquired using a magnetization-prepared rapid gradient-echo (MPRAGE) sequence with parameters: matrix size 256×256, resolution 1×1×1 mm³, and 208 slices.

The fMRI paradigm was used to locate the subject's sensorimotor areas related to hand movement. The paradigm consisted of two parts. The first part involved passive movement, where two experimenters assisted the subject with passive fist clenching on the left and right sides at a frequency of approximately 0.5 Hz. This was designed to test whether sensory information could be transmitted to the cortex, indicating the condition of the subject's ascending pathways. The second part involved motor imagery, where the subject was asked to imagine moving their left or right hand in a familiar manner. This was used to locate the hand motor areas in the primary motor (M1) and primary sensory (S1) cortices. The block design included two alternating conditions: movement and rest. At the beginning of the movement condition, an arrow pointing left or right appeared on the screen with a text prompt to "start imagining left hand/right hand movement." At the beginning of the rest condition, an image of a teacup appeared with a text prompt to "rest, relax, stay calm," instructing the subject to remain relaxed during this period. Each condition lasted 14 seconds (7 TRs, yielding 7 fMRI frames), repeated for 14 cycles. The left- and right-hand conditions alternated with a rest condition in between (Fig. S2).

S1.04 - Surgical Planning

Based on the results of the functional MRI activations, we developed a surgical implantation plan for the subject. Using the fMRI activation heatmaps combined with anatomical localization of the

hand motor and sensory areas, we performed 3D modeling to select specific sites on the precentral and postcentral gyri for the right hand, where epidural cortical electrodes were placed to cover regions of significant fMRI activation (Fig. S2). The internal device was implanted into the flat skull behind the ear, ensuring sufficient bone thickness, avoiding the temporalis muscle, and facilitating wireless powering.

To effectively integrate the electrode positioning from the surgical plan with the surgical navigation system, an image registration method was developed to address compatibility issues between the 3D model and the navigation system. The cortex was segmented using FreeSurfer¹, and an individualized cortical model of the patient's brain was constructed. The electrode placement on the cortical surface was designed in Blender to cover the functional areas of the precentral and postcentral gyri. To import the positioning results into the surgical navigation system, we wrote the electrode locations into the patient's original T1 DICOM data. This process involved coordinate transformation between FreeSurfer's Surface RAS reference frame and the image's original RAS reference frame (Equation 1).

$$X' = AX \quad 1$$

where X represents the homogeneous coordinates of the electrode points in the Surface RAS reference frame $(x, y, z, 1)$, X' represents the new coordinates in the original RAS reference frame (x', y', z') , and A is the transformation matrix (3×4) converting from the FreeSurfer's Surface RAS coordinate system to the DICOM image's scanner RAS coordinate system. An optimized KD-tree nearest neighbor algorithm was used to efficiently map these coordinates to the pixel points in the original DICOM images. In this setup, all pixels within a 1mm radius were marked with a value significantly higher than the maximum MRI intensity (e.g., 5000). The modified DICOM files were then imported into the navigation system, allowing the surgeon to directly determine the electrode positions during surgery. The final electrode implantation sites, as shown in Fig. 1d, matched the planned locations and the areas of optimal fMRI activation.

S1.05 - Impedance Measurement

The NEO system supports impedance measurement using milliampere (mA) stimulation current. The system uses a stimulation current of 1 mA with a pulse width of 1ms at a pulse frequency of 10 Hz for a duration of 5s. It measures the impedance between the epidural electrode contacts. Once a month, we record impedance data to track the trend of internal environment change (Fig. 2g).

S1.06 - Brain-Computer Interface Training Paradigms

The calibration task is utilized for personalized model calibration and BCI testing. The task consists of 15 trials per session, with each trial including 5 seconds of movement, feedback (10 seconds for success, 2 seconds for failure), and 5 seconds of resting state. The experiment begins with a 10-second period during which a crosshair appears at the center of the screen, and the participant needs to focus on the crosshair and remain calm. After 10 seconds, the actual task begins. At the start of the motor imagery task, a one second blank screen is firstly given to remind the participant to prepare. After that, an arrow pointing left or right appears at the center of the

screen, indicating left-hand or right-hand movement respectively, accompanied by a text prompt "Start imagining left-hand/right-hand movement." Feedback is provided after the motor phase, with the model making a judgment every second during the 5-second motor phase. The task has three difficulty levels: easy, medium, and hard, requiring correct judgments of 3, 4, and 5 times respectively. Only with correct judgments will the participant receive pneumatic hand feedback and a "Congratulations" message on the screen; otherwise, the message "Keep trying" will be displayed (Fig. S5a). Before fixing the model, random feedback with an 85% accuracy rate is given. In the first session of the calibration paradigm, fake feedback is used. In the second calibration session, feedback results are calculated using the model calibrated with the first session of training data. After the second calibration session, the final model is trained using data from both sessions and fixed for the patient. We perform this calibration task monthly to periodically assess the model's performance.

During rehabilitation training, the patient uses the fixed model for free grasping tasks. The model makes a judgment every 0.1 seconds to determine the patient's grasping or relaxation state. To avoid false triggers caused by the EEG offset response after the patient's releasing an object, there is a 3-second freeze period during which no new judgments are made. The model displays the confidence level of the grasp in the form of a progress bar on the screen, providing visual feedback to the participant. To quantitatively evaluate the effectiveness of the BCI system, we designed a **nine-square grid task**, requiring the patient to move objects to designated targets using the BCI actuated pneumatic glove. A 50.4 cm wide and 35.6 cm long nine-square grid board, as well as standard components of height 15 cm, upper cylinder diameter 4.5/6/6.5 cm, and lower disc diameter 10 cm were used in this paradigm (Fig. S5b). The patient is instructed by the experimenter to use the BCI to drive the pneumatic hand to grasp the standard component from the center of the nine-square grid and move it to the designated color block position, then release the object by controlling the pneumatic hand. The test is repeated in two rounds, and the total time from the start of the instruction to the successful placement of the object is recorded to evaluate whether the patient can smoothly control the state switching of the BCI system. We also compared the patient's success rate with and without BCI assistance. Success is defined as completing the task within 10 seconds without touching the grid boundaries before picking up the object and without dropping it midway. Any other result is considered a failure.

S1.07 – Daily Assessment Task

To monitor changes in signal quality over time, we designed a daily assessment task that records data during each data acquisition session. The test consists of 30 seconds of resting-state eECoG activity, followed by 15 elbow lifts (10 with the hand contralateral to the implant site and 5 with the ipsilateral hand), 15 imagined grasps (10 with the contralateral hand and 5 with the ipsilateral hand), and 15 pneumatic hand-driven passive movements (all with the contralateral hand). Each movement consists of 5 seconds of motion and 5 seconds of rest and is performed only once without repetition.

S1.08 – Deep Learning based Hand Trajectory Tracing

To accurately capture hand movement trajectories during the free grasping process, a USB webcam was positioned directly above the experimental table to record the hand movements from a top-down perspective (Fig. S9). A serial port synchronization signal and LED light were used to synchronize the video recording with the EEG data. For the video data of both pneumatic hand grasping and bare hand grasping, we finetuned a hand keypoint detection model to analyze the hand movement trajectories. The main structure of the model utilizes a high-resolution convolutional network (HRNet)² pre-trained on the OneHand10k dataset. The detection algorithm employs distribution-aware coordinate representation (DARK)³ based on heatmaps to detect four key points of the pneumatic hand or the bare hand: the index fingertip, thumb tip, the base of the thumb (thenar), and the wrist. For the patient's grasping data, the coordinates of the thenar key point were extracted as the hand movement trajectory. The start time of each trial was defined as the moment the hand contacted the central cylindrical object, and the end time was defined as the moment of grasping failure or successfully reaching the target position and releasing the object. The model was then fine-tuned based on the OneHand10K pre-trained model. The pneumatic hand model training data included 1,295 annotated images with a resolution of 960x540, with 80% of the data used for training and 20% for testing. The keypoint recognition model achieved an AUC of 0.89. The bare hand detection model training data included 1,118 annotated images with a resolution of 960x540, with 80% of the data used for training and 20% for testing. The model achieved an AUC of 0.85.

S2 – Riemannian Decoder

S2.01 - Spatio-Spectral Riemannian Geometry Decoding Method

The spatio-spectral information in epidural ECoG (eECoG) signals can be described using a covariance matrix. Typical eECoG responses to motor imagery include ERSP across different frequency bands. By constructing a multi-band joint covariance matrix (Equation 3), we can effectively extract the spatio-spectral patterns of the EEG:

$$C_f = \begin{pmatrix} Z_{f_1} Z_{f_1}^T & \dots & Z_{f_1} Z_{f_F}^T \\ \vdots & \ddots & \vdots \\ Z_{f_F} Z_{f_1}^T & \dots & Z_{f_F} Z_{f_F}^T \end{pmatrix} \quad 3$$

where $Z_{f_i}, i = 1, \dots, F$ represents the channel signals filtered by different frequency bands, and F is the number of selected frequency bands.

The Affine Invariant Riemannian Metric (AIRM, Equation 4)⁴ can measure the distance between covariance matrices:

$$\delta_r(C_1, C_2) = \left\| C_1^{-\frac{1}{2}} C_2 C_1^{-\frac{1}{2}} \right\|_F = \left(\sum_{i=1}^n \log^2 \lambda_i \right)^{\frac{1}{2}} \quad 4$$

where $\|\cdot\|_F$ represents the Frobenius norm, and λ_i are the eigenvalues of the matrix $C_1^{-1/2} C_2 C_1^{-1/2}$.

The AIRM metric has the following property: for any two samples from the source space that form covariance matrices S_A and S_B , mapping through a propagation matrix L (where L is invertible) results in sensor space covariance matrices $X_A = LS_A L^T$, $X_B = LS_B L^T$. It can be proven that:

$$\delta_r(X_A, X_B) = \delta_r(S_A, S_B)$$

This indicates that the separability in the source space and the sensor space is identical. Similarly, over long-term use, physiological changes may alter the propagation matrix L' , but the AIRM distance measure ensures that separability remains unchanged. In contrast, BCI decoding algorithms using spatial filters may fail due to changes in the propagation matrix, causing spatial filter templates to become ineffective. Therefore, BCI decoding algorithms using the AIRM metric possess robustness in the sensor space and long-term stability.

To select the most effective frequency bands for decoding, we evaluated the separability of different frequency bands for resting and right-hand motor imagery states using a Riemannian-based class distinctiveness method. Linear discriminant analysis (LDA) can be extended to construct class distinctiveness metrics under the Riemannian metric (Equation 5)⁵:

$$D(A, B) = \frac{\delta_r(\overline{C^A}, \overline{C^B})}{\frac{1}{2}(\sigma_{C^A} + \sigma_{C^B})} \quad 5$$

where \overline{C} represents the mean covariance under the Riemannian metric, and σ_C represents the standard deviation of the covariance under the Riemannian metric, $\sigma_C = \frac{1}{n-1} \sum_{i=1}^n \delta_r(C_i, \overline{C})$. The superscripts $C^{(A/B)}$ indicate the corresponding classes.

Subsequently, a classifier based on AIRM can be constructed by embedding the data into the tangent space⁶. For the manifold M constituted by the aforementioned eECOG feature covariance matrices, the Fréchet mean point X_{ref} of the manifold can be found (Equation 6):

$$X_{ref} = \operatorname{argmin}_{X_{ref}} \sum_{i=1}^N \delta^2(X_i, X_{ref}) \quad 6$$

Based on this point, the tangent space $T_{X_{ref}}M$ can be constructed, and the data points X_i can be embedded into this space to obtain the projected points S_i (Equation 7), where logm denotes the matrix logarithm operation.

$$S_i = \text{log}_{X_{ref}}(X_i) = X_{ref}^{-\frac{1}{2}} \text{logm} \left(X_{ref}^{-\frac{1}{2}} X_i X_{ref}^{-\frac{1}{2}} \right) X_{ref}^{-\frac{1}{2}} \quad 7$$

In our study, the epidural intracranial EEG of patients exhibits a typical event related synchronization (ERS) effect at high frequencies (e.g., 55-95Hz) and a typical event related desynchronization (ERD) effect at low frequencies (15-30Hz and 35-50Hz). Therefore, we designed a dual-frequency integrated spatio-spectral Riemannian geometry algorithm. Due to the physiological differences between low-frequency and high-frequency oscillatory activities, low-frequency activities were filtered at 15-30Hz and 35-50Hz, while high-frequency activities were band-pass filtered at 55-95Hz and then enveloped (Fig. S3). Subsequently, a large covariance matrix of the feature signals was constructed, which was whitened to retain 99% of the variance dimension components to reduce the dimensionality. The samples were then embedded into the tangent space constituted by the Fréchet mean point, and finally sent to a logistic regression classifier to build the decoder for BCI calibration.

S2.02 - Control Decoding Methods

We employed two classical BCI decoding methods to evaluate our model. **Linear Model:** To evaluate the decoding method proposed in this paper, we selected a commonly used linear model as a baseline for comparison^{7,8}. This linear model first uses a band-pass filter in the 0-150Hz frequency range to filter the signal into nine different frequency bands and then downsamples to 10Hz. The signals from the nine frequency bands and different channels are then concatenated into a 315-dimensional feature vector (7 channels * 9 frequency bands * 5 time points). Finally, this feature vector is used for decoding with a logistic regression classifier. 10-fold cross-validation is then used to optimize the regularization parameter of the logistic regression classifier to prevent overfitting. **Common spatial pattern (CSP) model:** Additionally, since there is a close relationship between Riemannian methods and spatial filtering methods, we designed a model using CSP spatial filters to compare with the Riemannian method^{9,10}. This model constructs the covariance matrix using the same frequency bands as the Riemannian method. The CSP method is then used to calculate and retain 16 spatial filters. The energy features of the resulting 16-dimensional spatial patterns are used for decoding with a logistic regression classifier. For each model, 10-fold cross-validation is used to optimize the regularization parameter of the logistic regression classifier to prevent overfitting.

S2.03 - Decoding Continuous Grasping States using Hidden Markov

Model

Considering that the natural grasping process is inherently continuous, with each state at a given time point being dependent on the preceding and following states, leveraging this dependency can significantly enhance the reliability of maintaining a grasp. The hidden Markov model (HMM), by constructing a multi-order stochastic process, links the probability of the current hidden state with the observed data and the probability of the hidden state at the previous time point. This can be used to describe the natural grasping process. We define the hidden states as either resting or grasping. In our constructed HMM algorithm, the emission probability $p(z_t|s_k)$ is derived from the Riemannian geometric classification model obtained through supervised training, while the transition probability matrix is semi-supervised, estimated using the forward-backward algorithm based on data from the patient's free-grasping training sessions. The first-order Hidden Markov Model can predict the probability of each hidden state at the current step based on the probability of each hidden state at the previous step (Equation 8):

$$p(s_{k,t}) = p(z_t|s_k) \sum_i p(s_{k,t}|s_{i,t-1})p(s_{i,t-1}) \quad 8$$

where z_t is the observed data at time t , and s_k is state k . We set a threshold p_{th} , and when the likelihood probability of the patient's new state exceeds this threshold, the model switches states. This threshold is estimated based on offline validation results and is set to 0.8 for the patient.

Additionally, we apply an extra step of first-order filtering to smooth the probabilities output by the HMM (Equation 9). The parameter η is adjusted based on offline validation results and is set to 0.7 for the patient.

$$\hat{p}_{curr} = \eta p_{last} + (1 - \eta)p_{curr} \quad 9$$

where p_{last} is the hidden state probability from the previous step, p_{curr} is the current hidden state probability inferred from Equation 6, and \hat{p}_{curr} is the final estimated hidden state probability.

S2.04 - Model Training and Evaluation

The model is trained based on two sets of calibration data. Since high gamma (HG) activity decays over time during imagined grasping, we use data from the first 1.5 seconds after the onset of motor imagery and the entire 5 seconds of resting state as the training data. The data are segmented at 0.5-second intervals for model fitting. One set of data is used for model training, utilizing 10-fold cross-validation to select the optimal regularization parameters for the classifier. After fitting the classification model, we fit the HMM state transition matrix using the patient's grasping behavior data to construct a complete decoding model. Validation is conducted using a

different set of data, evaluating both segment metrics and event metrics. After validation, a final model is trained using both sets of calibration data.

During model calibration, it is necessary to design evaluation criteria to assess the effectiveness of the model. Since the goal is to decode natural grasping states, which is a continuous time process, evaluation needs to consider both segment metrics (such as sample classification accuracy) and event metrics (sensitivity and specificity of event detection). **Segment Metrics:** The model directly classifies data segments and calculates classification accuracy. Additionally, due to the uneven distribution of classes in the segmented data samples, the F1 score (the harmonic mean of precision and recall) is used, which is insensitive to class imbalance. For segment metrics, the random level for the F1 score and AUC is 0.5. **Event Metrics:** To evaluate grasping accuracy over continuous time, we designed event-based metrics. If a grasping event is correctly identified within 0.5s before its onset and 2 seconds after it, it is considered a correct decision; otherwise, it is a false negative. If more than one grasping event is detected during a single grasping event, it is considered a false positive. Precision, recall, and their harmonic mean (F1 score) are calculated accordingly. Due to the low frequency of grasping events, the random level for event metrics is low. Monte Carlo simulations estimate the random level for the F1 score of event metrics to be approximately 0.09 (with the grasping onset time covered about 10% of total time), indicating that continuous grasping tasks are relatively difficult, much harder than simple binary classification tasks.

S3 - Offline Analysis of EEG/ECoG data

S3.01 - Comparison of Three Types of Brain Electrophysiology

Recordings

To compare the differences between epidural electrocorticography (eECoG) and subdural electrocorticography (sECoG), we utilized data from the publicly available Kai Miller dataset¹¹. Since the motor imagery patterns of paralyzed patients are more similar to actual movements in healthy individuals¹², we selected real hand movement data from 10 patients whose electrodes covered the hand area. The cortical electrodes in the Kai Miller dataset had a spacing of 10 mm and a contact diameter of 2.3 mm. In our study, we used electrodes with a spacing of 8 mm and a contact diameter of 3.2 mm, which are comparable in size. The EEG electrode spacing in the patients' EEG caps was approximately 4 cm. To ensure consistent results, all three types of brain electrical activity were processed using the common average re-reference method. Additionally, to study the spatial resolution differences between different brain recordings, we introduced motor imagery data from the BCI2000 dataset for comparison¹³.

In terms of frequency, we calculated the event-related spectral perturbation (ERSP) for eECoG, sECoG, and EEG during the 0-2.5 seconds of movement relative to the 0-2.5 seconds of resting state (Equation 2). This allowed us to compare the modulation depths of different frequency bands across the different brain electrical activities.

$$ERSP = \frac{P_{task} - P_{rest}}{P_{rest}} \quad 2$$

Where P_{task} refers to the power of the brain electrical activity in the frequency band during movement, and P_{rest} refers to the power in the resting state. Power spectral density (PSD) was calculated using resting state data to compare the spectral energy differences of the different brain electrical activities (Fig. 2b).

To qualitatively compare the spatial resolution differences, we calculated the relationship between the distance between electrode pairs and the correlation coefficient of the electrode signals (Fig. 2c). To maintain consistency with the number of subjects and tasks selected in the eECoG dataset, we selected all electrode pairs from the first 10 subjects in the BCI2000 dataset for real left- and right-hand movements. All eECoG signals were filtered with a 1 Hz high-pass filter, using the original reference electrodes (EEGs were referenced to mastoids, sECoGs and eECoGs were referenced to the scalp).

S4 – Electrophysiological and Neuological Assessment of Rehabilitation

S4.01 – SEP Measurement

The testing of somatosensory evoked potentials (SEP) follows the standards of the international federation of clinical neurophysiology (IFCN)¹⁴. The stimulation sites are at the wrist corresponding to the median, radial and ulnar nerves respectively. A 6×9 cm silver/silver chloride adhesive electrode is used. The positive electrode is placed distally on the trunk, the negative electrode proximally, with a 2 cm distance between them. The stimulation is a unidirectional pulse, with 2 Hz frequency 400 μs pulse width and amplitudes of 16 mA for the median and radial nerves, or 12 mA for the ulnar nerve. This setup aims to stably evoke SEP while avoiding pain. The stimulation is repeated 160 times in each session. During stimulation, SEPs are recorded with epidural electrodes of NEO BCI system at a sampling rate of 1000 Hz. The signals are band-pass filtered (20-400 Hz), baselined according to the average of 90 ms data before stimulation onsets, and averaged across trials to obtain the SEP waveform. Monthly recordings are repeated at the same stimulation site and parameters to observe changes in the SEP waveform.

In SEP analysis, for early (15-35 ms¹⁵) and late (40-80 ms¹⁶) SEP components, the average absolute amplitude is extracted¹⁷. To minimize amplitude increases due to enhanced random phase oscillatory activity, the Bootstrap method is used. For each Bootstrap sample set, the average SEP response is extracted, and the average waveform amplitudes of early and late components are extracted. For the data from 1st and 9th month after implantation, permutation test is used to calculate the p-values that 9th month's amplitude is greater than that of 1st month, and the FDR correction is applied to control the false discovery rate in multiple comparisons.

S4.02 – Neurological Scales Measurement

This study uses the international standards for neurological classification of spinal cord injury (ISNCSCI) scale¹⁸ and the action research arm test (ARAT) scale¹⁹ to assess patients' neurological and upper limb functional status, respectively. The ISNCSCI scale is evaluated by two attending physicians, and any discrepancies in their evaluations are discussed to reach a single result. The ISNCSCI scale is measured monthly starting from the 2nd to 9th month post-surgery. The ARAT scale assessments are conducted by rehabilitation physicians and experimenters, with the process being video recorded (Video 2).

Supplemental Figures

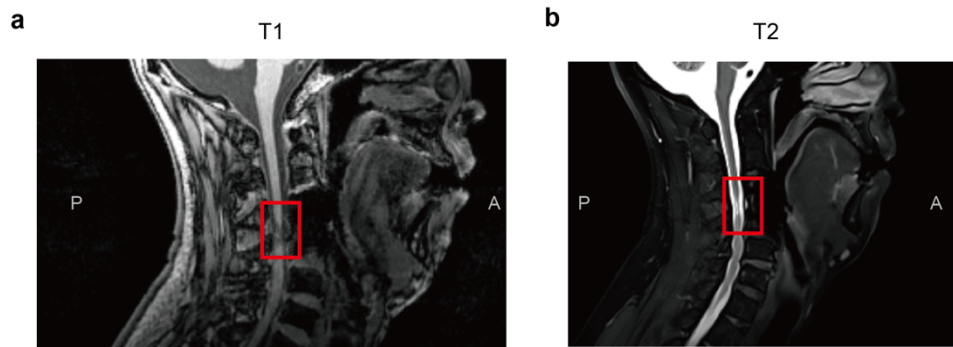


Figure S1 MRI Scans of the Patient's Head and Neck.

a, Cervical spine T1 structural image b, Cervical spine T2 structural image; the red box indicates the location of the patient's spinal cord injury.

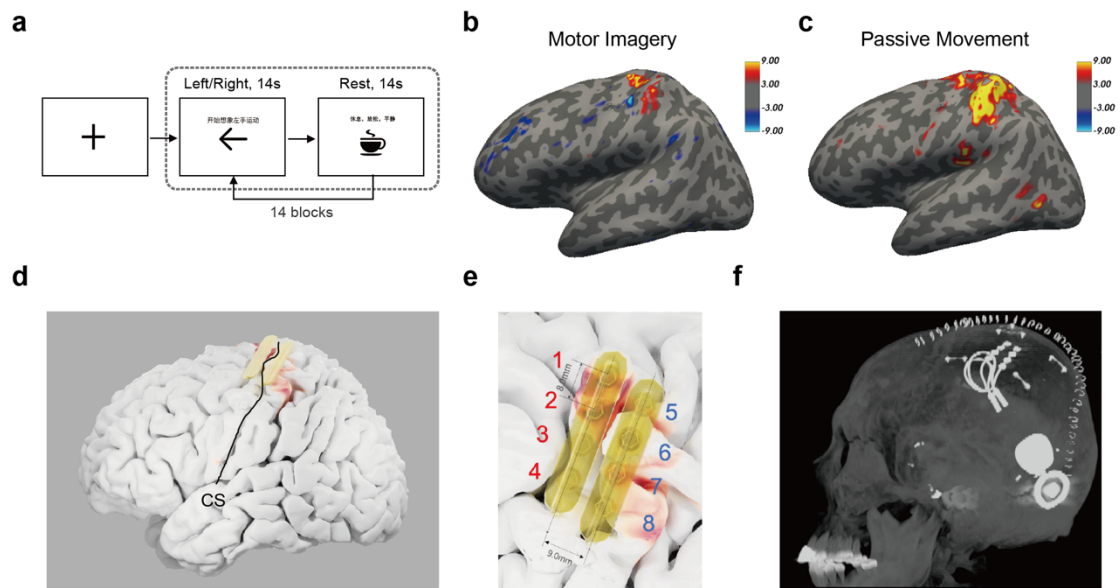


Figure S2 fMRI Localization Task and Surgical Planning.

a, fMRI functional localization task, including alternating rest and movement states of the left or right hand. b-c, Functional activation during motor imagery (b) and passive movement (c), with activation values represented as $-lg(p)$. d, Electrode planning. e, Enlarged view of the diagram of the planned electrodes. Electrodes 1-4 were located on the precentral gyrus and electrodes 5-8 on the postcentral gyrus. f, Sagittal View of postoperative CT, showing the actual implantation positions. CS: Central Sulcus.

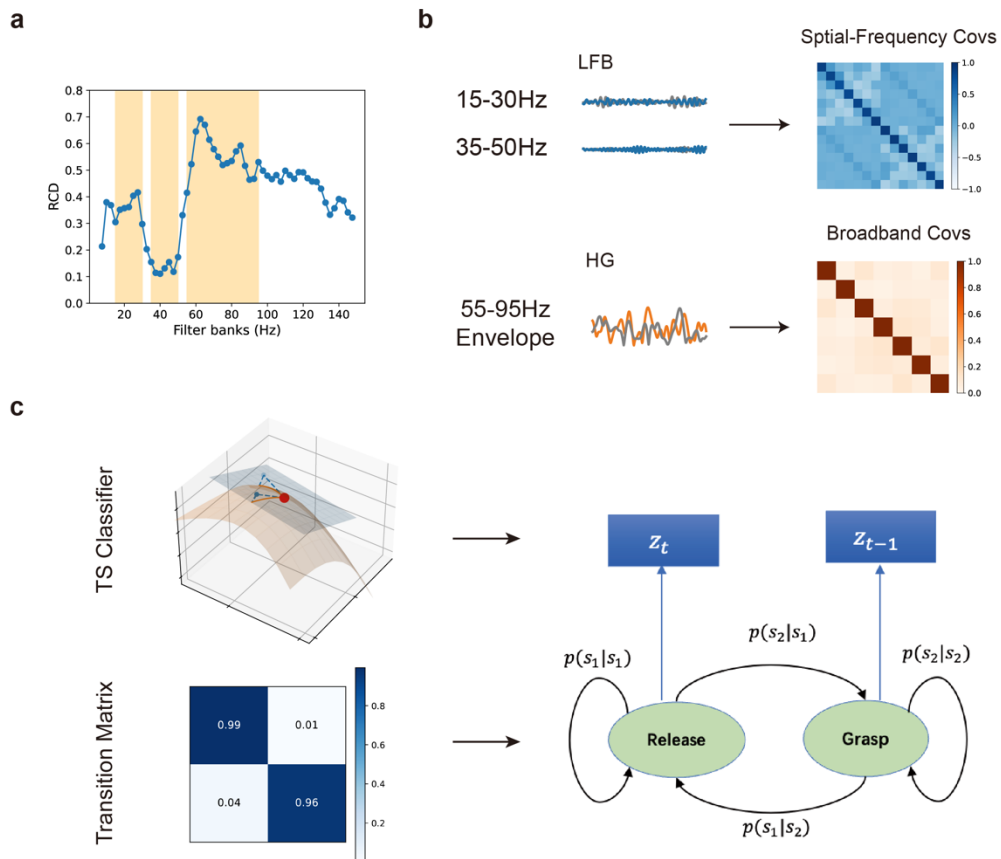


Figure S3 Brain-Computer Interface Decoding Methods.

a, Band selection using Riemannian class distinctiveness (RCD) across different frequency bands. b, Construction of the covariance feature matrix using low-frequency band-pass filter features and high-frequency envelope features. c, Decoding framework for natural grasping based on the hidden Markov model (HMM), utilizing the temporal dependence of grasp states to ensure the reliability of continuous grasping. The observation model is based on the trained Riemannian geometry classifier, and the transition matrix is fitted based on patient behavior data. TS Classifier: Tangent Space Classifier.

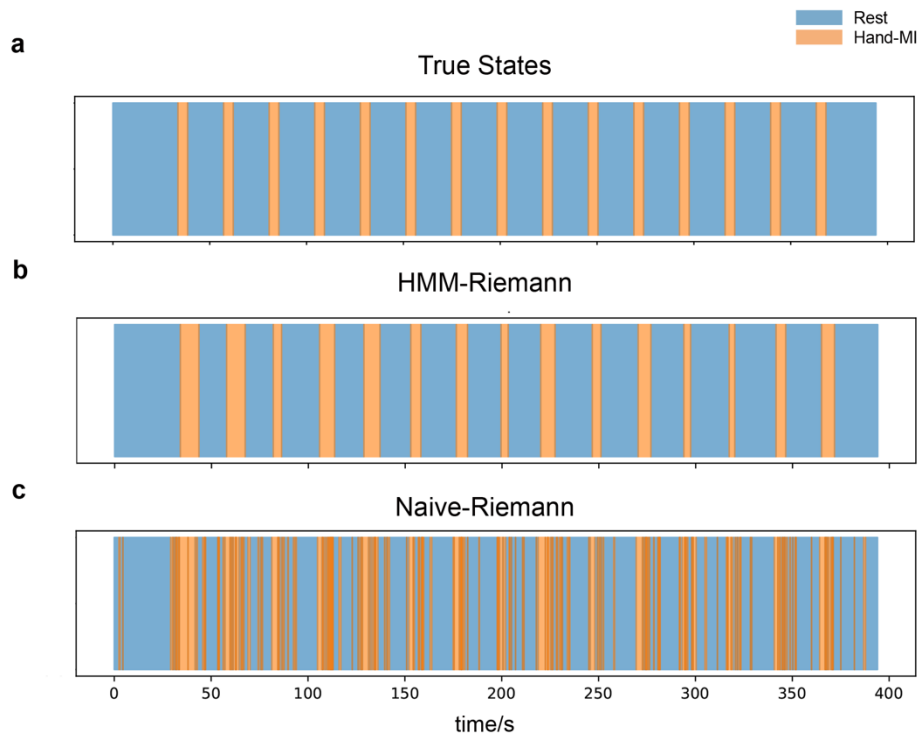


Figure S4 Illustration of HMM decoding.

a, Actual motor imagery cues. b, Continuous grasping decoded by the HMM-Riemann method. c, Continuous grasping decoded by the Naïve-Riemann method without HMM. Hand-MI: Hand Motor Imagery.

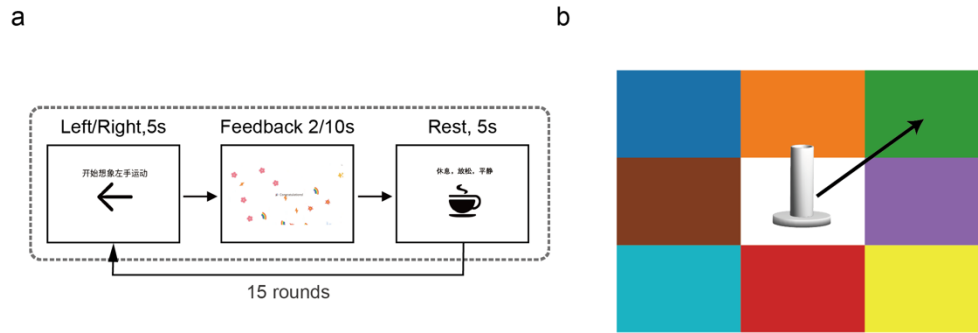


Figure S5 Calibration and Training Paradigms.

a, BCI calibration paradigm. b, Free grasp BCI testing task, where the patient needs to move the standard cylinder from the central grid (in white) to one of the eight peripheral grids (in color) designated by the experimenter.

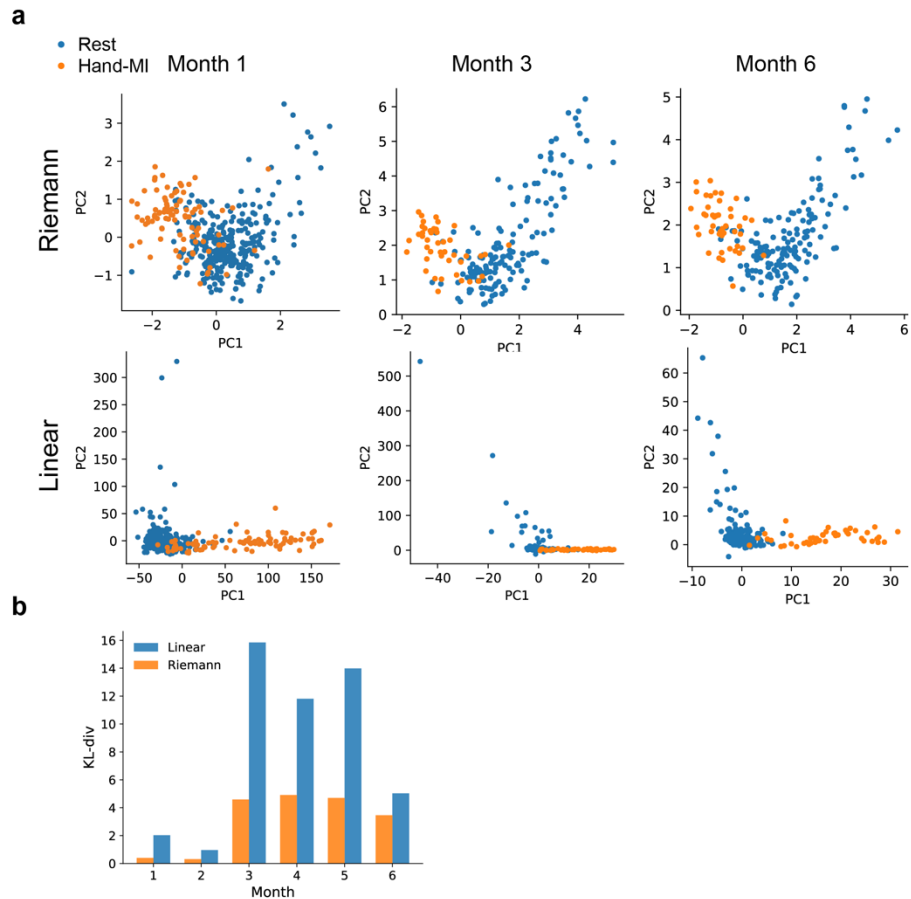


Figure S6 Evolution of epidual ECoG Feature Distribution During Long-term Use.

a, Scatter plots of PCA-embedded distributions of Riemannian features and linear spatio-temporal-spectral features across different months. b, Changes in KL divergence between Riemannian features and linear spatio-temporal-spectral features compared to training data over different months. The stability of Riemannian features consistently surpasses that of linear spatio-temporal-spectral features. Hand-MI: Hand Motor Imagery. KL-div: KL Divergence.

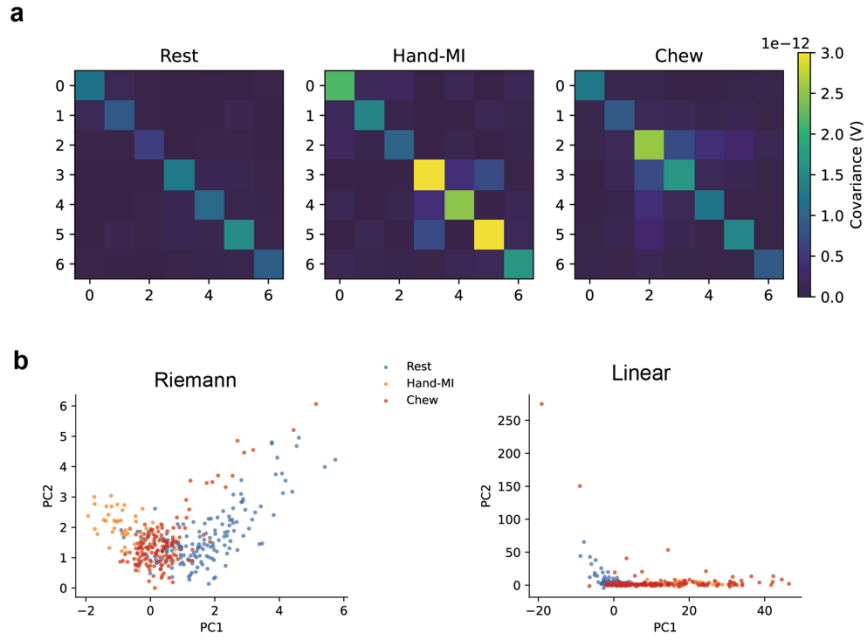


Figure S7 EMG Noise Pattern.

a, Average covariance patterns of resting, motor imagery (Hand-MI), and EMG noise. b, Dimensionality-reduced spatial distribution patterns of Riemannian embedded features (left) and linear spatio-temporal-spectral features (right). Under Riemannian metrics, chewing EMG noise is positioned between resting and hand motor imagery; in linear spatio-temporal-spectral features, chewing noise highly overlaps with hand motor imagery distribution.

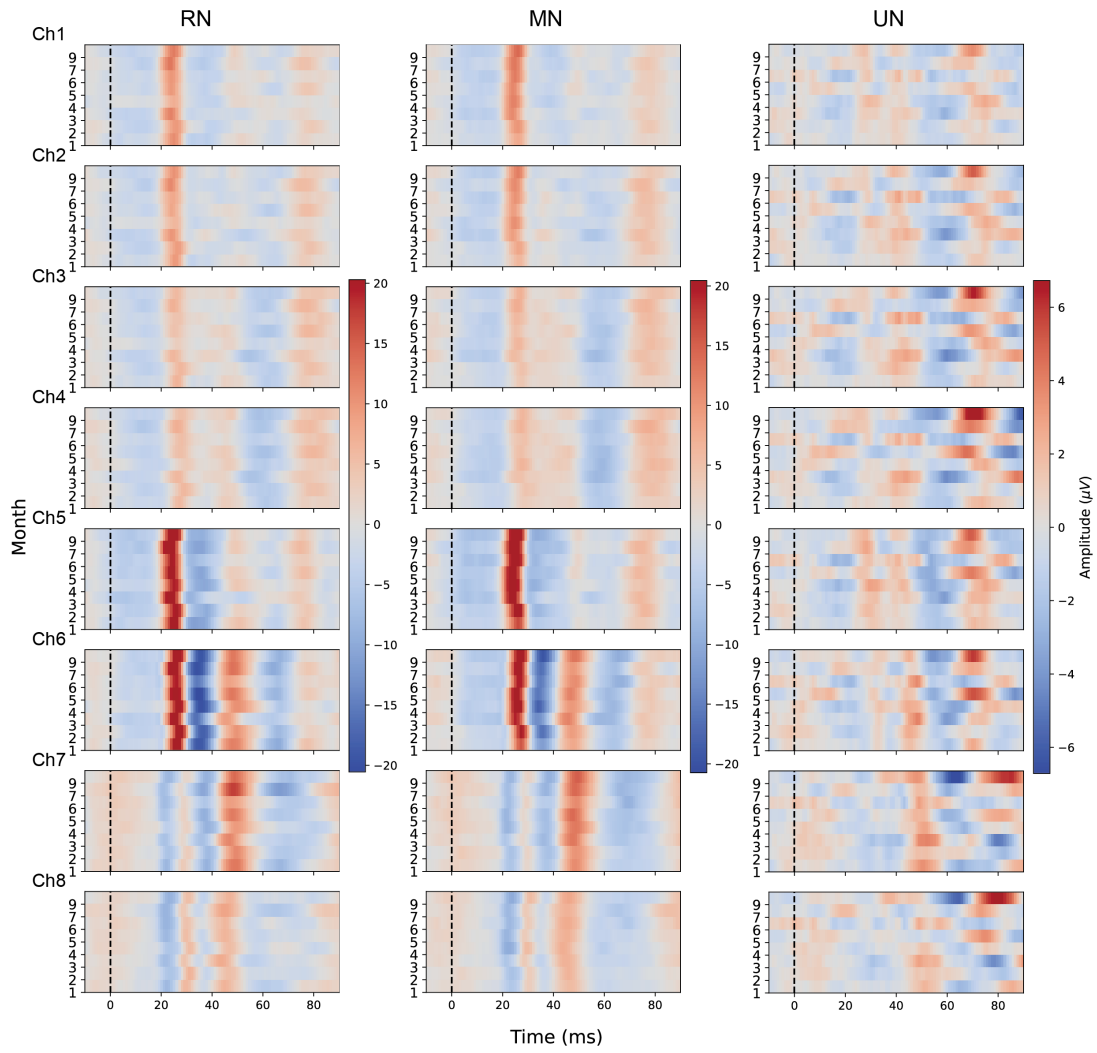
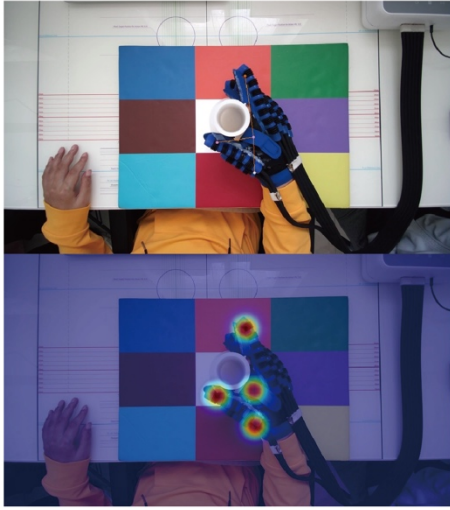
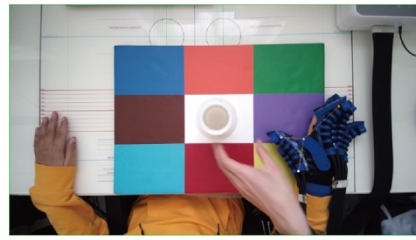


Figure S8 Average Somatosensory Evoked Potential (SEP) Waveforms.
Average SEPs for Each Nerve, Channel, and Month. From top to bottom: Ch1-Ch8.

a



b



c



Figure S9 Pneumatic Hand Keypoint Detection Model.

a, Example of a detection heatmap. b-c, Examples of detection results.

Supplemental Tables

Table S1: ISNCSCI Scores

Time	Pre-Operation (Day -4)	Month 3 (Day 78)	Month 4 (Day 129)	Month 5 (Day 162)	Month 6 (Day 198)	Month 7 (Day 234)	Month 9 (Day 279)
American Spinal Injury Association Impairment Scale (AIS)	A	A	A	A	A	A	A
Neurological level of injury	C4	C4	C4	C4	C4	C4	C4
Upper Extremity Motor Score							
C5, (Left Right)	4 4	4 4	4 5	4 5	4 5	4 5	5 5
C6, (Left Right)	3 3	3 3	3 3	3 4	3 3	3 3	3 4
C7, (Left Right)	2 2	2 2	2 3	2 2	2 2	2 3	2 3
C8, (Left Right)	0 0	0 0	0 0	0 0	0 0	1 0	0 1
T1, (Left Right)	0 0	0 0	0 0	0 0	0 0	0 0	0 0
Total, (Left Right)	9 9	9 9	9 11	9 11	9 10	10 11	10 13
Light Touch Sensory Score							
Total, (Left Right)	7 8	9 7	8 9	11 9	7 7	7 7	7 7
Pin Prick Sensory Score							
Total, (Left Right)	6 7	10 8	10 8	11 8	10 9	11 10	11 11
Deep Anal Pressure	No	No	No	No	No	No	No
Voluntary Anal Contraction	No	No	No	No	No	No	No

Table S2: p-values for Increases in Average Amplitudes.

	RN		MN		UN	
	Early	Late	Early	Late	Early	Late
Ch1	0.2461	0.0901	<0.0001	0.0746	0.1579	0.0069
Ch2	0.2369	0.2654	<0.0001	0.1905	0.3035	0.0007
Ch3	0.2555	0.0479	0.0235	0.0119	0.2198	<0.0001
Ch4	0.1068	0.0021	0.0396	0.0381	0.1161	<0.0001
Ch5	0.0078	0.9957	<0.0001	0.1021	0.2586	0.0013
Ch6	0.5814	0.9572	<0.0001	<0.0001	0.1724	<0.0001
Ch7	0.3704	0.184	0.0176	<0.0001	0.3169	0.0001
Ch8	0.3518	0.9889	<0.0001	0.0001	0.2373	<0.0001

Compared between SEP data from month 1 and month 9 of Early and Late SEP Components for Different Nerves.

Table S3: ARAT Scores

	Baseline (Day 15)		Month 3 (Day 77)		Month 5 (Day 147)		Month 7 (Day 204)		Month 9 (Day 280)	
	L	R	L	R	L	R	L	R	L	R
Grasp (18)	6	4	5	6	6	10	6	9	12	13
Grip (12)	6	6	6	6	6	6	6	6	7	10
Pinch (18)	2	2	2	2	4	4	3	4	5	6
Gross (9)	7	9	8	9	8	8	8	8	8	8
Total (57)	21	21	21	23	24	28	23	27	32	37

Table S4: Training Sessions

Session	Post-Implant Day	Time/Hr	Calibration	Training	Assessment
1	15	1.5		Daily	ARAT
2	21	1.5		Daily	
3	23	1		Daily	
4	25	2		Daily	
5	27	1.5	CA	Daily	
6	29	2	CA	Daily, FG	
7	31	2	CA	Daily, FG	
8	35	2.5	CA	Daily, FG	
9	37	2.5	CA	Daily, NG	SEP
10	39	1.5	CA	Daily, NG	
11	41	1.5	CA	Daily, NG	
12	43	1.5	CA	Daily, NG	
13	45	1		Daily	
14	49	1		Daily	
15	53	1.5		Daily	
16	55	2		Daily	
17	57	1.5		Daily	
18	63	2		Daily	
19	65	2		Daily	SEP
20	71	1		Daily, NG	

21	73	1		Daily, FG	
22	77	2		Daily	ARAT
23	78	1.5			ASIA
24	79	1.5		Daily, NG	
25	83	1.5		Daily, FG	
26	87	1.5		Daily, FG, NG	
27	91	2		Daily	
28	93	1.5		Daily, FG	SEP
29	96	1		Daily, FG	
30	97	1		Daily, FG	
31	99	0.5		Daily	
32	119	1.5	CA	Daily, FG	
33	121	2		Daily, FG, Other	
34	126	1.5	CA	Daily, NG, Other	
35	127	2.5		Imp, Other	
36	129	1.5		-	ASIA
37	133	2		Daily, NG, FG	
38	135	1		Daily, NG, FG	
39	139	1		Daily, NG, FG	
40	141	1.5		Daily, NG	
41	143	1.5		Daily, NG, FG	
42	147	1.5		Daily, NG	
43	149	1		Daily, NG, FG	

44	153	2	CA	Daily, NG, FG	
45	155	2		Daily, NG, FG, Other	
46	157	2		Daily, NG, FG	SEP
47	161	1.5		Daily, NG, FG	
48	162	1.5			ASIA
49	167	1.5		Daily, NG, FG	
50	169	2		Daily, NG, FG	
51	171	1.5		Daily, NG	
52	177	1.5		Daily, NG, FG, Imp	
53	181	1.5	CA	Daily, NG, FG	
54	183	1		Daily, NG, FG	
55	185	2		Daily, NG, FG	SEP
56	189	1		Daily, NG, FG	
57	191	1		Daily, NG	
58	195	1.5		Daily, NG, FG	
59	197	1.5		Daily, NG	
60	198	1.5			ASIA
61	200	1.5		Daily, NG, FG	
62	203	1.5		Daily, NG	
63	205	1.5			ARAT
64	209	1		Daily, NG, FG	
65	211	1	CA	Daily, NG, FG, Imp	

66	213	1		Daily, NG, FG	
67	217	1.5		Daily, NG	SEP
68	220	0.5		Daily, NG, FG	
69	223	1		Daily, NG, FG	
70	225	1		Daily, NG	
71	227	1.5		Daily, NG, FG	
72	231	1.5		Daily, NG	
73	233	2		Daily, NG	
74	234	1.5			ASIA
75	237	1		Daily, NG, FG	
76	239	1.5		Daily, NG, FG	
77	240	1.5		Daily, NG, FG	
78	241	3		Daily, Other	
79	244	1.5		Daily, Other	
80	245	1.5	CA	Daily, NG, FG, Other	
81	246	1.5		Daily, NG, FG, Other	
82	247	1.5	CA	Daily, NG, FG, Other	
83	248	1		Daily, NG, FG	
84	251	2		Daily, NG, FG	
85	252	1		NG, FG	
86	253	1.5		Daily, NG, Other, Imp	
87	254	1		NG, FG, Other	

88	255	1		Daily, NG, FG, Other	
89	258	1		Daily, NG, FG, Other	
90	259	1		NG, FG, Other	
91	260	1.5		Daily, NG, FG, Other	
92	261	1.5		NG, FG, Other	
93	262	1.5		Daily, NG, FG, Other	
94	265	1.5		Daily, NG, FG, Other	
95	266	1		NG, FG, Other	
96	267	1		NG, FG, Other	SEP
97	268	1		Daily, NG, FG, Other	
98	269	2.5		Daily, NG, FG, Other	
99	272	1		NG, FG, Other	
100	273	1		Daily, NG, FG, Other	
101	274	1		NG, FG, Other	
102	275	1.5		Daily, NG, FG, Other	
103	276	1.5		NG, FG, Other	
104	279			Daily, Other	ASIA
105	280				ARAT
106	282				SEP

Abbreviations:

Daily: Daily assessment test

CA: Calibration task

FG: Free grasping task

NG: Nine-grid grasping task

Imp: Impedance test

Other: Other training tasks

Reference

1. Fischl, B. FreeSurfer. *Neuroimage* **62**, 774–781 (2012).
2. Wang, J. *et al.* Deep High-Resolution Representation Learning for Visual Recognition. *IEEE Trans. Pattern Anal. Mach. Intell.* **43**, 3349–3364 (2021).
3. Zhang, F., Zhu, X., Dai, H., Ye, M. & Zhu, C. Distribution-Aware Coordinate Representation for Human Pose Estimation. *Proc. IEEE Comput. Soc. Conf. Comput. Vis. Pattern Recognit.* 7091–7100 (2020) doi:10.1109/CVPR42600.2020.00712.
4. Congedo, M., Barachant, A. & Bhatia, R. Riemannian geometry for EEG-based brain-computer interfaces; a primer and a review. *Brain-Computer Interfaces* **4**, 155–174 (2017).
5. Yamamoto, M. S., Lotte, F., Yger, F. & Chevallier, S. Class-distinctiveness-based frequency band selection on the Riemannian manifold for oscillatory activity-based BCIs: preliminary results. in *2022 44th Annual International Conference of the IEEE Engineering in Medicine & Biology Society (EMBC)* vols 2022-July 3690–3693 (IEEE, 2022).
6. Barachant, A., Bonnet, S., Congedo, M. & Jutten, C. Classification of covariance matrices using a Riemannian-based kernel for BCI applications. *Neurocomputing* **112**, 172–178 (2013).
7. Benabid, A. L. *et al.* An exoskeleton controlled by an epidural wireless brain-machine interface in a tetraplegic patient: a proof-of-concept demonstration. *Lancet Neurol.* **18**, 1112–1122 (2019).
8. Moly, A. *et al.* An adaptive closed-loop ECoG decoder for long-term and stable bimanual control of an exoskeleton by a tetraplegic. *J. Neural Eng.* **19**, (2022).
9. Koles, Z. J. The quantitative extraction and topographic mapping of the abnormal components in the clinical EEG. *Electroencephalogr. Clin. Neurophysiol.* **79**, 440–447 (1991).
10. Lemm, S., Blankertz, B., Curio, G. & Müller, K. R. Spatio-spectral filters for improving the classification of single trial EEG. *IEEE Trans. Biomed. Eng.* **52**, 1541–1548 (2005).
11. Miller, K. J. A library of human electrocorticographic data and analyses. *Nat. Hum. Behav.* **3**, 1225–1235 (2019).
12. Lotze, M. & Halsband, U. Motor imagery. *J. Physiol. Paris* **99**, 386–395 (2006).
13. Schalk, G., McFarland, D. J., Hinterberger, T., Birbaumer, N. & Wolpaw, J. R. BCI2000: A General-Purpose Brain-Computer Interface (BCI) System. *IEEE Trans. Biomed. Eng.* **51**, 1034–1043 (2004).
14. Cruccu, G. *et al.* Recommendations for the clinical use of somatosensory-evoked potentials. *Clin. Neurophysiol.* **119**, 1705–1719 (2008).
15. Allison, T., McCarthy, G., Wood, C. C. & Jones, S. J. Potentials evoked in human and monkey cerebral cortex by stimulation of the median nerve. A review of scalp and intracranial recordings. *Brain* **114**, 2465–2503 (1991).
16. Allison, T., McCarthy, G. & Wood, C. C. The relationship between human long-latency somatosensory evoked potentials recorded from the cortical surface and from the scalp. *Electroencephalogr. Clin. Neurophysiol. Evoked Potentials* **84**, 301–314 (1992).
17. Jorge, A. *et al.* Area under the Curve of Somatosensory Evoked Potentials Detects Spinal Cord Injury. *J. Clin. Neurophysiol.* **36**, 155–160 (2019).
18. Rupp, R. *et al.* International standards for neurological classification of spinal cord injury. *Top. Spinal Cord Inj. Rehabil.* **27**, 1–22 (2021).
19. Yozbatiran, N., Der-Yeghiaian, L. & Cramer, S. C. A standardized approach to performing the

action research arm test. *Neurorehabil. Neural Repair* **22**, 78–90 (2008).